J Mol Model (2013) 19:4433–4441
DOI 10.1007/s00894-013-1955-0

ORIGINAL PAPER

Molecular dynamics simulation of temperature induced unfolding of animal prion protein

Xin Chen · Danhui Duan · Shuyan Zhu · Jinglai Zhang

Received: 11 May 2013 / Accepted: 22 July 2013 / Published online: 8 August 2013

Abstract To elucidate the structural stability and the unfolding dynamics of the animal prion protein, the temperature induced structural evolution of turtle prion protein (tPrPc) and bank vole prion protein (bvPrPc) have been performed with molecular dynamics (MD) simulation. The unfolding behaviors of secondary structures showed that the α-helix was more stable than β-sheet. Extension and disruption of β-sheet commonly appeared in the temperature induced unfolding process. The conversion of α-helix to π-helix occurred more readily at the elevating temperature. Furthermore, it was suggested in this work that the unfolding of prion protein could be regulated by the temperature.

Keywords Elevated temperature · Molecular dynamics (MD) simulation · Prion protein · Unfolding

Introduction

Transmissible spongiform encephalopathies (TSEs), or prion diseases, are neurodegenerative disorders characterized by a spongiform neurodegeneration of the brain caused by prions [1–3]. This group of diseases includes Creutzfeldt-Jakob disease (CJD), Kuru in humans, as well as sheep scrapie and bovine spongiform encephalopathy (BSE) [4–6]. The pathogenic mechanisms of prion diseases are diverse, while the conformational conversion of the normal cellular prion protein (PrPc) into the scrapie isoform (PrPsc) is a central etiological event [5, 7]. The two isoforms of prion protein can be distinguished by the composition of their secondary structure: PrPc was about 42 % helical with a very low (~3 %) β-sheet content, whereas PrPsc contains of 30 % α-helices and 43 % β-sheets [8–10]. The conversion of PrPc into PrPsc includes an obvious conformational transition of secondary structure. Then the kinetics of the unfolding of PrPc is essential to the understanding of the molecular pathogenesis of prion diseases. The unfolding time of PrPc is varied from μs to ms, which is too hard to simulate using direct MD simulation [11, 12]. Recently, many acceleration factors of protein folding have been studied, such as the pH value, pressure, temperature and hydrodynamics. It has been found that the misfolding of human prion protein involves a partial unfolding and misfolding step as PrP converts to a PrPsc-like structure rich in extended structure at low pH [13–15]. Flow molecular dynamics (FMD) simulation was another recommendable technique to probe the protein unfolding with the shear flow [16, 17]. Chen et al. has investigated the flow induced structural transition in the β-switch region of glycoprotein Ib by generating stable water flow under constant temperature [18]. Protein denaturation at high temperature and pressure was of interest for understanding the mechanism of protein conformational change [19, 20]. Okumura has performed a multibaric-multithermal MD simulation of a 10-residue protein to dissect the difference of the mechanism between temperature denaturation and pressure denaturation [21]. Pure high-temperature simulations were also used to bring about the unfolding of the globular domain. Particularly, it has been found that the unfolding of protein could be accelerated by temperature without changing the unfolding pathway [22–24].

The determination of the tertiary structure of protein was important for the dynamics study of prion protein. So far, many prion proteins have been determined by the nuclear magnetic resonance (NMR) [25, 26] and X-ray diffraction (XRD) analysis [27, 28]. It has provided structural insights into the molecular basis of prion disease. However, the tertiary structure of PrPsc is still absence. Then the study of the misfolding mechanism from PrPc to PrPsc is focused on the unfolding dynamics of PrPc. Moreover, it is difficult to obtain the complete and specific dynamic information of proteins

X. Chen (✉) · D. Duan · S. Zhu · J. Zhang (✉)
Institute of Environmental and Analytical Sciences, College of Chemistry and Chemical Engineering, Henan University, Kaifeng 475001, Henan, China
e-mail: xin_chen@henu.edu.cn
e-mail: zhangjinglai@henu.edu.cn

with the limitation of experimental conditions and detection limit. Molecular dynamics (MD) simulation has become one of the most important methods to study the structural evolution, as it could both provide plentiful dynamics information and model the required environment for structural conversion easily. It has been successfully applied to explore how the mutation, pressure, temperature and pH affect the conversion between PrPc to PrPsc [29–31].

To gain more insights into the molecular basis of the prion diseases, temperature involved unfolding of animal prion protein was studied by the MD simulation. The turtle prion protein (tPrPc) and the bank vole prion protein (bvPrPc) were selected to study the thermo-stability and the dynamics motion of prion protein. Turtle is one of the few mammalian species that appear to be resistant to TSE and the bank vole is often used as an animal model of the study on prion protein [32, 33]. It is expected to reveal the pathogenic mechanism of prion diseases from the structural and mechanical properties of protein, as well as to provide ideas to the therapy of prion diseases.

Methods

System setup

The initial structures of tPrPc and bvPrPc were obtained from the protein data bank (PDB) and the PDB entries were 1U5L [25] and 2K56 [26], respectively (Fig. 1). Missing hydrogen atoms were added using the AUTOPSF plug-in of VMD [34]. The purified proteins were immersed in a water box with TIP3P [35] model water molecules. Periodic boundary conditions were employed with a solvent shell of 10 Å. The water box was selected to be large enough to accommodate the structural changes during the MD procedures. And the volume of the water boxes of tPrPc and bvPrPc were 72.58×61.66×56.76 $Å^3$ and 72.50×57.80×48.09 $Å^3$, respectively. And two sodium ions were added to neutralize the two systems, respectively. The weakly acidic environment was simulated with all titratable side chains charged.

Molecular dynamics preparation

In this study, all MD simulations were performed with NAMD version 2.7 [36] using Charmm27 force filed [37]. The production MD phase was carried out with a time step of 2 fs and the van der Waals (VDW) interaction was truncated at 10 Å. The long-range electrostatic interactions were calculated using the particle mesh Ewald (PME) summation scheme. During the MD simulation, the Langevin method was turned on to control the constant pressure at 101.3 kPa. Energy minimization was performed to optimize the geometry of the two protein molecules and then MD simulation was applied to equilibrate each system for 10 ns.

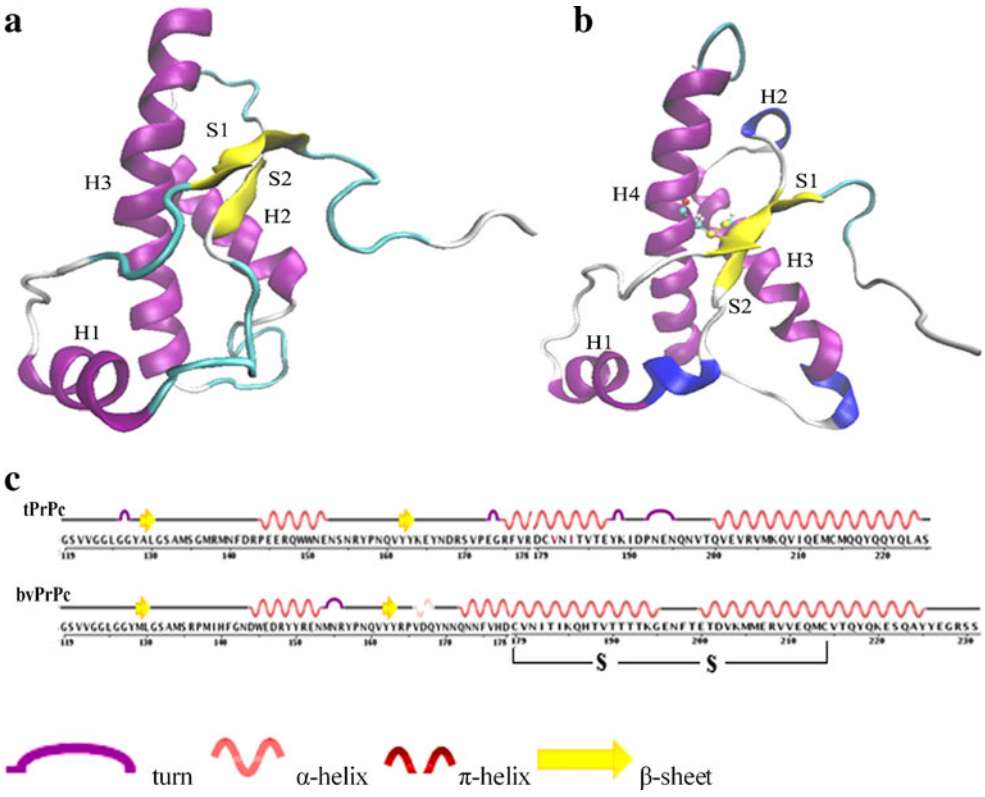

Fig. 1 Schematic ribbon diagrams of **a** tPrPc and **b** bvPrPc and **c** primary sequence of the two proteins

Initialization of temperature

The elevated temperature about 500 K was often used to study the temperature induced fast unfolding of protein [38–40]. In order to clarify the temperature dependent unfolding mechanism and investigate the unfolding dynamics of animal prion proteins, a series of lower temperatures were introduced in this work. In addition to the elevated temperatures, the body temperature of 310 K was used as a reference. Then five temperatures of 310 K, 373 K, 423 K, 473 K and 523 K with the interval of 50 K were selected.

Analytical methods

Time evolutions of root mean square deviation (RMSD), root mean square fluctuation (RMSF), hydrophobic and hydrophilic solvent accessible surface areas (SASA) [41], side chain-side chain contacts [14, 42], and secondary structures during the simulations were calculated with the Timeline plug-in of VMD. The trajectories were also analyzed with VMD. And SASA was calculated with the probe radius of 1.4 Å.

Results and discussion

Structural deviations

RMSD of the backbone atoms (N-C_α-C) with respect to the simulation time of tPrPc and bvPrPc at different temperatures were shown in Fig. 2a and b, respectively. The various RMSD fluctuations resulted by the different given temperatures were discerned in the graph. As shown in Fig. 2a, it could be found that the RMSD fluctuations were enlarged with the increase of temperatures. However, the RMSD curve at 310 K was overlapped by that at 373 K during the last 5 ns. The RMSD of tPrPc was increased with the elevating temperature. While in the bvPrPc system, the curves were classified into three groups with the RMSD value. The curve of 310 K was overlapped by that of 373 K before 6.0 ns, and the curves of 423 K and 473 K were staggered in the whole simulation. The three curves of 373 K, 423 K and 473 K were twisted together from 8.7 ns to 10.0 ns. The RMSD of 523 K was obviously larger than that of all the lower temperatures. As H3 and H4 were bridged by the disulfide bond, the fluctuation of H3 and H4 in bvPrPc was constrained. Furthermore, the fluctuation amplitude of RMSD in tPrPc system was larger than that in bvPrPc system. The RMSD response to the temperature of tPrPc was more sensitive than that of bvPrPc at elevated temperature, which showed that the thermostability of bvPrPc was greater than that of tPrPc.

Structural fluctuations

The RMSF of the two proteins was displayed in Fig. 3 to gain insight into the structural fluctuation. The tPrPc was composed of three α-helices and two β-strands. And they were donated as H1 (Arg143—Asn153), H2 (Gly174—Tyr188), H3 (Thr199—Ser225), S1 (Ala129—Leu130) and S2 (Tyr162—Tyr163), respectively. The three α-helices, one 3_{10}-helix and two β-strands of bvPrPc were named as H1 (Asn143—Met154), H2 (Pro165—Tyr169), H3 (Asn171—Glu196), H4 (Thr199—Tyr226), S1 (Met129—Leu130) and S2 (Tyr162—Tyr163), respectively. And a disulfide bond between Cys179 and Cys214 was formed to bridge the H3 and H4 in the bvPrPc system (Fig. 1).

Except for the two peaks of C-terminal and N-terminal, there were three notable peaks in the RMSF graph of tPrPc (Fig. 3a). And the three peaks were found to be resulted by the flexibility of the loop structures. And the three loops were named as t-loop1 (between S1 and H1), t-loop2 (between S2 and H2) and t-loop3 (between H2 and H3), respectively. In addition to the large fluctuation of the two terminus of tPrPc, two notable plateaus in the RMSF graph were resulted by the fluctuation of t-loop2 and t-loop3, which was also found in the previous MD studies of human prion protein [3, 43]. The steady-state ^{15}N{^{1}H}-NOEs of bovine prion protein also showed that the loop between the second and the third α-helices was the most flexible region [44]. The RMSF at 523 K was obviously larger than that at lower temperatures, however, the RMSF curves of the other three elevated temperatures was

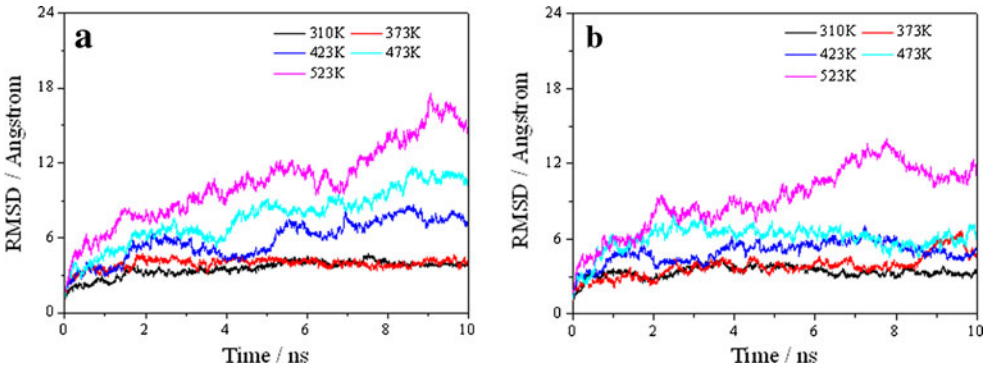

Fig. 2 Evolution of RMSD of the backbone atoms (N-C_α-C) during 10 ns simulations at different temperatures. **a** tPrPc; **b** bvPrPc

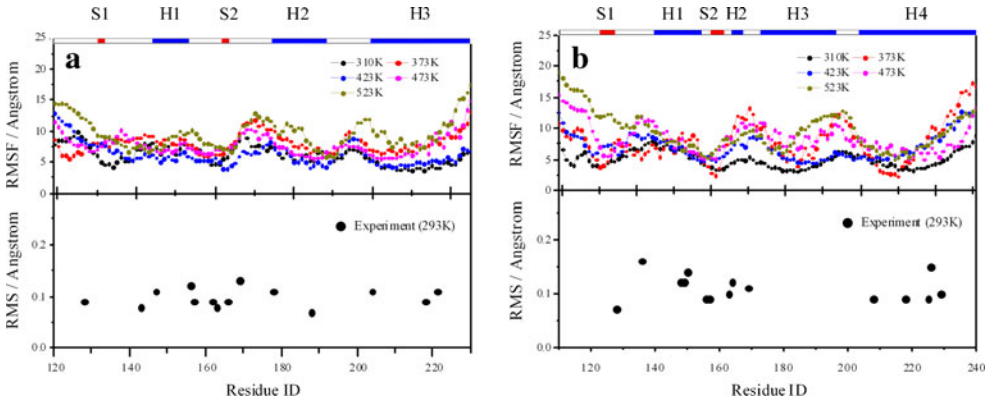

Fig. 3 RMSF of the MD structures and experimental RMS values as a function of residue number. The β-sheets and α-helices were displayed with red bars and blue bars, respectively. **a** tPrPc; **b** bvPrPc

twisted together with that of 310 K. With the increase of temperature, the peak of t-loop1 was widened by the unfolding of S1 and H1. With the unfolding of H2, the peak of t-loop2 was gradually heightened and widened. The H3 was the most rigid helix, and the peak of t-loop3 was hard to widen until the temperature was elevated to 523 K. The experimental RMS data of some residues of tPrPc were also displayed in Fig. 3a [25], it was found that the fluctuation trend of RMSF obtained in this study was coincided with the experimental RMS values.

The three notable peaks in Fig. 3b were corresponding to bv-loop1 (between S1 and H1), bv-loop2 (between H2 and H3) and bv-loop3 (between H3 and H4). It was found that all three peaks were enlarged at the elevated temperature, which showed that the structural flexibility of bvPrPc was sensitive to the temperature. The peak of bv-loop3 was obviously widened at 523 K, which resulted from the unfolding of H3. It was also found from Fig. 3b that the fluctuation trend of RMSF was well coincided with the experimental RMS of bvPrPc [26].

Secondary structure evolution

Unfolding of β-sheet

The final state of the secondary structure (α-helix and β-sheet) at different temperature in the tPrPc system was listed in Table 1. The content of the rigid secondary structure of the original state was also listed as a reference. It was discerned from the table that elevated temperature was effective in unfolding the protein. It had been found that β-sheet was more active than α-helix. As shown in Table 1, the β-sheet at the final state was preserved at 310 K and extended at 373 K. To gain more insight into the dynamics of β-sheet, the percentage of β-sheet of tPrPc during the simulation at different temperature was shown in Fig. 4. It could be found that the preservation of the β-sheet listed in Table 1 at 373 K was an accidental result. The elongation, partial and complete unfolding of β-sheet were common activities appearing during the whole MD procedure. With the increase of temperature, the unfolding behavior became predominant. Except for 423 K, the increase of β-sheet occasionally appeared at the other four temperatures. However, the extension of β-sheet was more readily appeared at 523 K and the total existing time of the elongation state of β-sheet was 492 ps. To discern the obvious loss of β-sheet at 423 K in Fig. 4c, the distances of hydrogen bonds (H-bonds) formed between the two strands of β-sheet at 373 K and 423 K were displayed in Fig. 5a and b, respectively. Two H-bonds of Ala219-Tyr163 and Gly131-Val161 were involved in the formation of β-sheet in tPrPc. At

Table 1 Content of the secondary structure of tPrPc at the end of the simulation

T/K	Helix 1	Helix 2	Helix 3	Sheet
Origin	143–153	174–188	199–225	129–130,162–163
310	143–152	174–188	199–222	129–130,162–163
373	143–153	174–187	199–223	130–133,160–163
423	143–153	174–187	201–222	–
473	143–151	175–180	202–210, 213–223	–
523	–	179–183	198–218	–

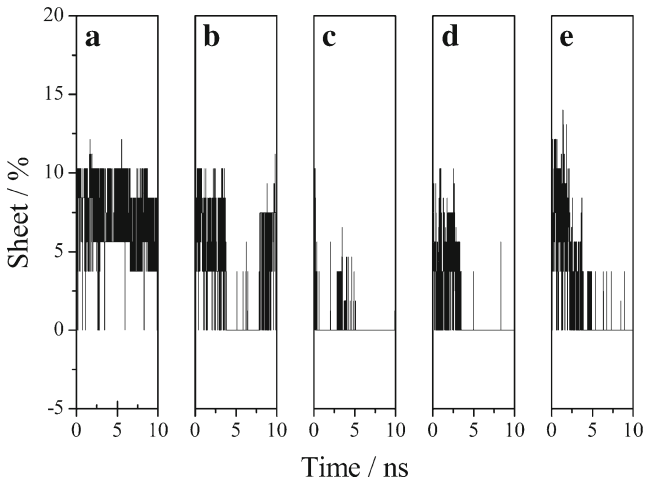

Fig. 4 Percentage of secondary structure (Sheets) in tPrPc system with respect to MD simulation. **a** 310 K; **b** 373 K; **c** 423 K; **d** 473 K; **e** 523 K

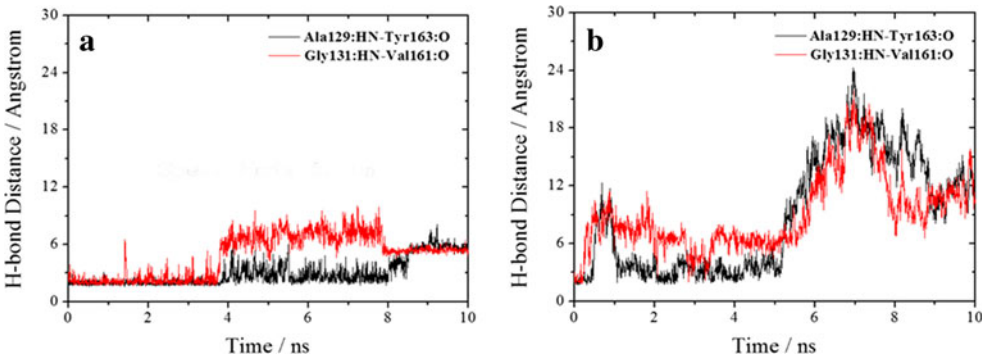

Fig. 5 Time evolutions of H-bonds involved in the formation of β-sheet in tPrPc at **a** 373 K and **b** 423 K

373 K, both the two H-bonds were stable under 3.0 Å before 3.8 ns. Yet the distance of Gly131-Val161 reached a plateau about 7.5 Å at 4.0 ns and sustained for 3.8 ns. Then it dramatically decreased to 5.0 Å and kept stable to the end of simulation. The Ala219-Tyr163 distance gradually climbed to a plateau of 6.0 Å. However, the two H-bonds were rather unstable at 423 K. The two curves increased rapidly to 12.0 Å before 1.0 ns and then the distances of Ala219-Tyr163 and Gly131-Val161 dropped to about 3.0 and 6.0 Å, respectively. Another peak of the two H-bonds at 423 K occurred from 5.0 ns to 9.0 ns. With the analysis of MD trajectory at 423 K, it was found that the strand 1 (residues 129–130) of β-sheet turned over with the unfolding of sheet, and it was hard to turn back, which led to the complete unfolding of β-sheet occurring in tPrPc at 423 K.

The unfolding dynamics of β-sheet was discerned in Fig. 6. The yellow belts of β-sheet at 310 K existed during the whole MD time. Yet they lost from 4.0 ns to 8.0 ns at 373 K and they even disappeared from 0.24 ns to 10 ns at 423 K. The extension of the yellow belts obviously occurred before 2.3 ns at 523 K. The high activity of β-sheet has been widely found in the wild-type and the mutated prion protein. For example, the elongation of β-sheet was found to be facilitated in valine variants and to be inhibited in proline variants [23]. It was also found in Chen's work that the multiple early misfolding pathways for the mutated PrPc were composed of the elongation, disruption and conversion of β-sheet to α-helix [45]. Both experimental and computational studies have observed the increasing of β-sheet structures during both acid-induced and heat-induced PrPc denaturation processes [13, 14, 46–49]. The extension of β-sheet and the formation of new β-sheet were found to occur more readily in low pH environments [14, 50].

Unfolding of the α-helix

As shown in Table 1, helix was stable enough to keep intact at elevated temperatures. H1 was the shortest helix and it was connected with flexible loops. Then the structure of H1 was held by the loops and not easily unfolded. It was found in the table that H1 was partly unfolded at 310 K and 473 K, however, it was completely unfolded at 523 K with the violent thermal motion. H2 began unfolding since the temperature was increased to 373 K. H3 was located at the terminal of tPrPc, the residues Leu223, Ala224 and Ser225 were readily to be unfolded. The unfolding of H3 might occur in the middle of helix column, and then two short rigid helices were bridged with the loop (473 K).

Further structural evolution of tPrPc during the simulation at different temperatures was shown in Fig. 6. It could be clearly found that the β-sheet (yellow) was active and prone to be unfolded at the elevated temperature. Yet the magenta α-helix showed more stability and not easily unfolded. In addition to the occasionally unfolding of the terminus of α-helix, the magenta belts of helix were kept intact in the whole MD process at 310 K. The terminal residues Ser225, Ala224 and Leu223 were transformed from helix to coil. The H-bond formed between Tyr221 and Ser225 was broken with the thermal motion. A conversion of turn (Asp191-Asn195) to π-helix occurred from 0 ns to 2.5 ns. With the increasing of the temperature, the unfolding of helix occurred more readily. The temperature-induced unfolding motion of tPrPc was found to begin from the end to the middle. For the long helix structure, the unfolding might appear simultaneously both in the end and the middle. During the unfolding procedure, the α-helix was transformed to turn (cyan), coil (white) and π-helix (red). And the conversion of α-helix to π-helix mostly occurred at high temperature, such as 473 K and 523 K. Furthermore, the original unfolding order of helix was similar at different temperature, which showed that the temperature was an effective method to probe the unfolding behavior of protein.

For the bvPrPc system, the contents of α-helix at different temperature were illustrated in Fig. 7. The content of helix was gradually decreased with the elevation of temperature, which showed that temperature could be used to regulate the unfolding rate of prion protein in the molecular simulation. A series of unfolding states of bvPrPc at 523 K were displayed in Fig. 8. And it could be found that the unfolding of β-sheet was also common in the bvPrPc system. While the unfolding

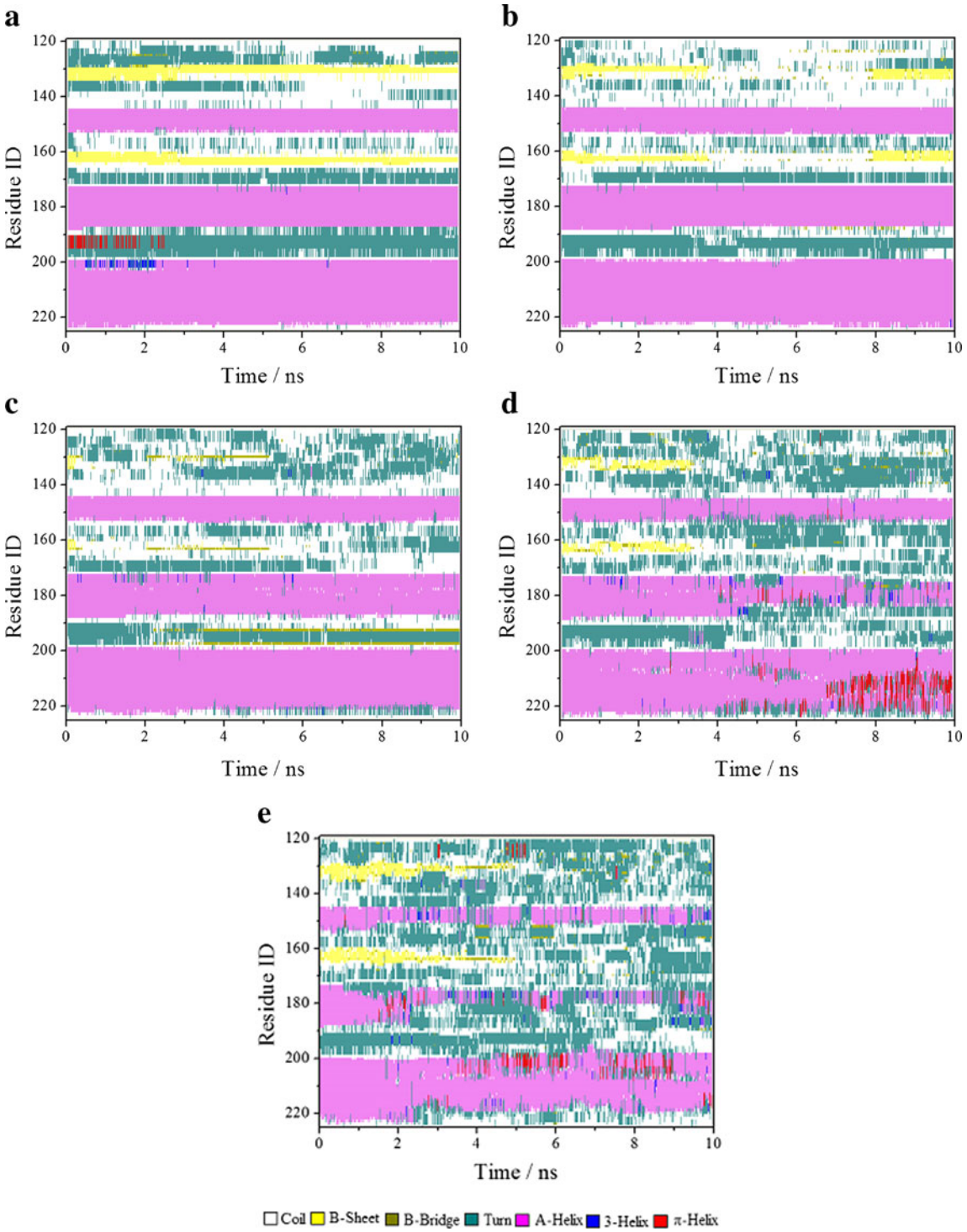

Fig. 6 Secondary structure evolutions as functions of time. **a** 310 K; **b** 373 K; **c** 423 K; **d** 473 K; and **e** 523 K. The assignments of secondary structures were made with VMD

of α-helix occurred in a stepwise manner. With the accelerating of high temperature, the α-helix was transformed to 3_{10}-helix (blue), π-helix (red), and turn (cyan). H3 and H4 was bridged by the disulfide bond (Cys179—Cys214), then the fluctuation of the two helices was restrained. Meanwhile, the unfolding of the H2 was also affected.

Surface areas

The time evolutions of hydrophobic and hydrophilic solvent accessible surface areas (SASA) were illustrated in Fig. 9. The hydrophobic SASA (S_{pho}) was increased with the unfolding of protein. On the contrary, the hydrophilic SASA (S_{phi}) was

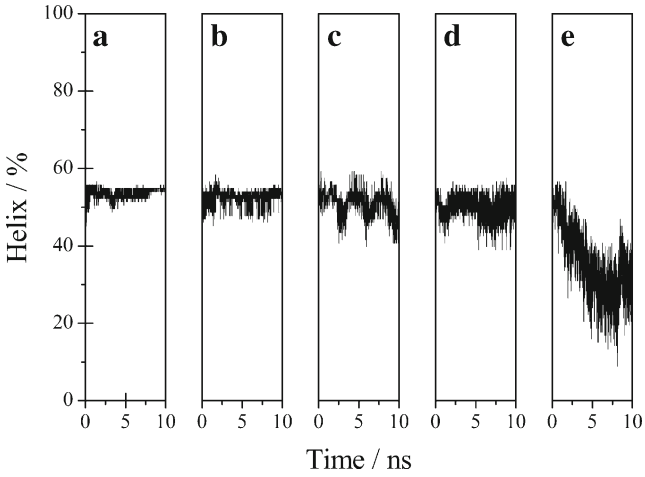

Fig. 7 Percentage of helix of bvPrPc with respect to time at **a** 310 K; **b** 373 K; **c** 423 K; **d** 473 K; **e** 523 K

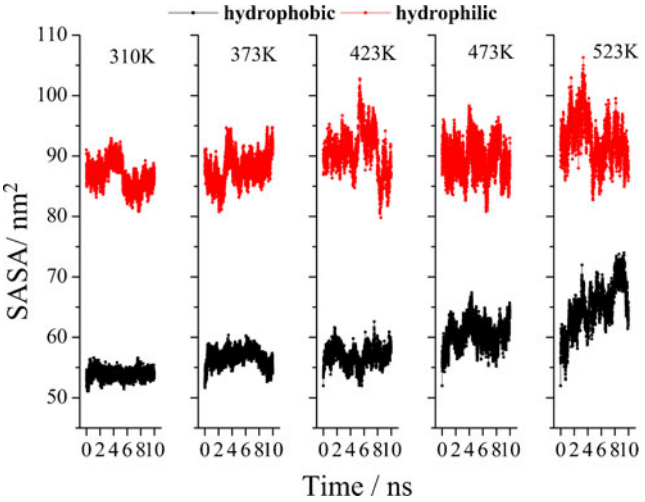

Fig. 9 Time evolutions of the hydrophobic SASA (*black*) and hydrophilic SASA (*red*) of tPrPc at different temperatures

decreased during the simulation. For example, the S_{pho} of tPrPc was changed from 56.33 nm^2 to 64.42 nm^2, and the S_{phi} of tPrPc varied from 93.27 nm^2 to 86.41 nm^2 at 523 K. The conversion tendency of S_{phi} and S_{pho} were consistent with the study on human prion protein [14]. As we know, the hydrophobic residues and side chains of protein were prone to be wrapped in the core, while the hydrophilic part was exposed to be compatible with aqueous solution. The unfolding of protein released the hydrophobic residues. And the hydrophobic effect resulted in the further increase of S_{pho}. For the hydrophilic residues of protein, they were found to be close to each other with H-bond and electrostatic interaction. Then the S_{phi} was dramatically fluctuated with the unfolding and misfolding of protein at the elevated temperatures. It was suggested that the denaturation of the protein involved an increase of the exposure of hydrophobic surfaces. And the same results could be found in the bvPrPc system.

Residue-residue contact map

The unfolding of the secondary structure resulted in the unpacking of the tertiary structure. The contact between different secondary structures was diminished during the simulation. Regions I and IV in Fig. 10 indicated that the β-sheet was unfolded with the disconnecting of the two strands. The change in region II of tPrPc showed that the contact between H1 and H3 was removed. In region III, the contact of H2 and H3 was diminished at the end of the simulation. However, the contact points of H3 and H4 was preserved in region V at the final state of bvPrPc. The difference was resulted by the disulfide bond in bvPrPc system.

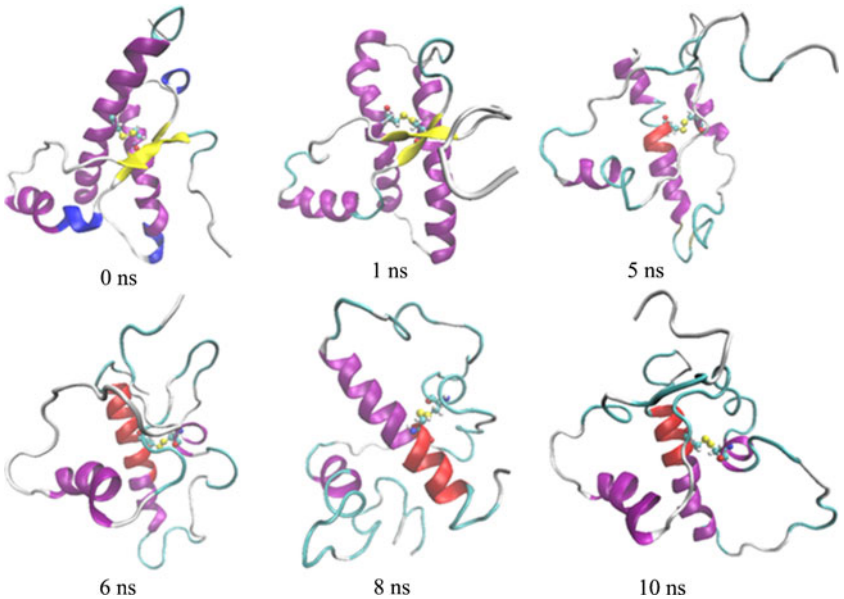

Fig. 8 Snapshots of the unfolding state of bvPrPc at 523 K from 0.0 ns to 10.0 ns. The α-helix, β-sheet, π-helix, coil and turn was colored in *magenta*, *yellow*, *red*, *white* and *cyan*, respectively. The water molecules were not shown for clarity

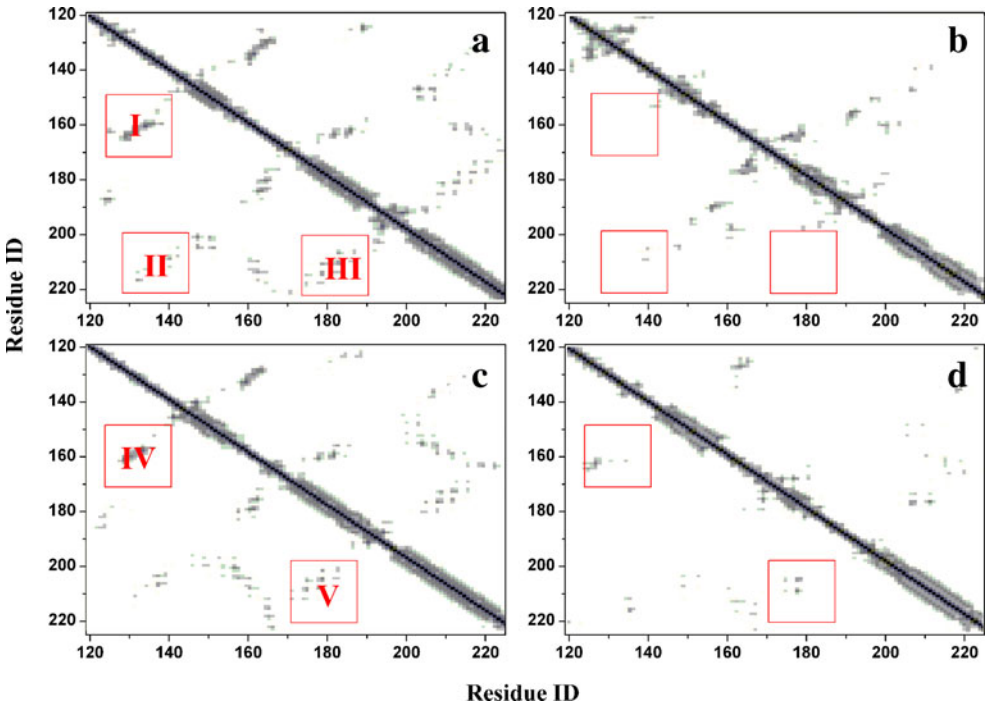

Fig. 10 Residue-residue contact maps for the representative conformation of the two proteins at 523 K. The initial state (**a**) and the final state (**b**) of tPrPc were shown in the top graphs. The initial state (**c**) and final state (**d**) of bvPrPc were shown in the bottom graphs

Unfolding of the two proteins at 523 K

The structural evolution of the two proteins at 523 K was similar. As shown in Fig. 11, the percentage of helix was reduced from 52.21 % to 25.66 % in the bvPrPc system. And it was changed from 46.72 % to 19.62 % in the tPrPc system. There was no sheet preserved for both systems at the end of simulation. The rigid helix and sheet were prone to transform to the turn. And it was increased by 22.43 % and 19.47 % after the simulation in tPrPc and bvPrPc, respectively. The percentage of coil was shown to be kept stable before and after the MD simulation. Except for the disulfide bond in bvPrPc, the composition of the secondary structures of the two homogenous proteins is similar, which was shown in Fig. 1c. Then the temperature induced unfolding of the two proteins might be helpful to discern the static and dynamics stability of different species of animal prion protein.

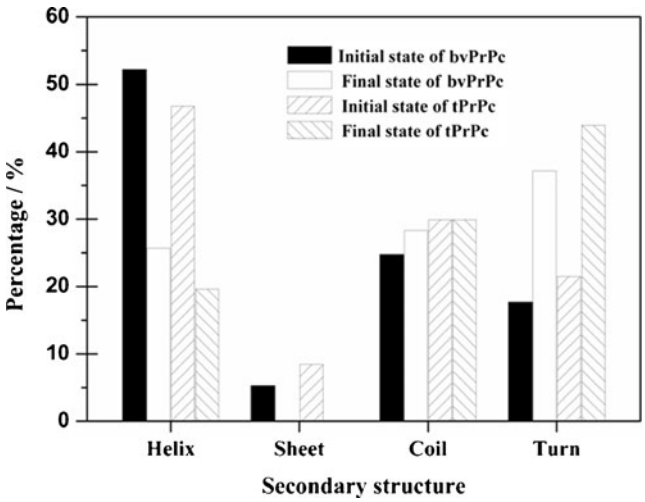

Fig. 11 Percentage of the main secondary structures at the initial and the final state of the two prion proteins at 523 K

Conclusions

By performing the all-atom MD simulation at different temperatures, the unfolding mechanism of tPrPc and bvPrPc were studied to understand the molecular basis of disease-related structural transition. It was found that the β-sheet was rather active with the elongation and disruption during the simulation. And the unfolding of β-sheet occurred more readily at the elevated temperature. The unfolding dynamics of α-helix was shown to begin from ends to the middle, and then the whole helix was unfolded. And the conversion of α-helix to π-helix was found to be common at the elevated temperature. The unfolding order of the secondary structure at different temperature was similar. Moreover, the unfolding extent of protein was increased with the elevation of temperature. It could be concluded that the elevating temperature could be used as the temperature probe to regulate the unfolding of prion protein.

Acknowledgments This work was financially supported by the National Natural Science Foundation of China (Grant No. 21003037) and the National Science Foundation of the Education Department of Henan Province (13A150085).

References

1. Prusiner SB (1996) Trends Biochem Sci 21:482–487
2. Weissmann C (1996) FEBS Lett 389:3–11
3. Rossetti G, Giachin G, Legname G, Carloni P (2010) Proteins 78:3270–3280
4. Caughey B, Chesebro B (2001) Adv Virus Res 56:277–306
5. Prusiner SB (1982) Science 216:136–144
6. Prusiner SB (1998) Proc Natl Acad Sci USA 95:13363–13383
7. Aguzzi A, Polymenidou M (2004) Cell 116:313–327
8. Stahl N, Baldwin MA, Teplow DB, Hood L, Gibson BW, Burligname AL, Prusiner SB (1993) Biochemistry 32:1991–2002
9. Caughey BW, Dong A, Bhat KS, Ernst D, Hayes SF, Caughey WS (1991) Biochemistry 30:7672–7680
10. Pan KM, Baldwin M, Nguyen J, Gasset M, Serban A, Groth D, Mehlorn I, Huang Z, Fletterick RJ, Cohen FE (1993) Proc Natl Acad Sci USA 90:10962–10966
11. Daggett V (2002) Acc Chem Res 35:422–429
12. Rathore N, Yan QL, de Pablo JJ (2004) J Chem Phys 120:5781–5788
13. Swietnicki W, Petersen R, Gambetti P, Surewicz WK (1997) J Biol Chem 272:27517–27520
14. Gu W, Wang T, Zhu J, Shi Y, Liu H (2003) Biophys Chem 104:79–94
15. DeMarco ML, Daggett V (2007) Biochemistry 46:3045–3054
16. Jaspe J, Hagen SJ (2006) Biophys J 91:3415–3424
17. Szymczak P, Cieplak M (2011) J Phys Condens Matter 23:033102–033115
18. Chen Z, Lou J, Zhu C, Schulten K (2008) Biophys J 95:1303–1313
19. Chara O, Grigera JR, McCarthy AN (2007) J Biol Phys 33:515–522
20. Perezzan R, Rey A (2012) J Chem Phys 137:185102–185111
21. Okumura H (2012) Proteins 80:2397–2416
22. Day R, Bennion BJ, Ham S, Daggett V (2002) J Mol Biol 322:189–203
23. Shamsir MS, Dalby AR (2005) Protiens 59:275–290
24. Wang T, Wade RC (2007) J Chem Theory Comput 3:1476–1483
25. Calzolai L, Lysek DA, Perez DR, Guntert P, Wuthrich K (2005) Proc Natl Acad Sci USA 102:651–655
26. Christen B, Perez DR, Hornemann S, Wuthrich K (2008) J Mol Biol 383:306–312
27. Apostol MI, Sawaya MR, Cascio D, Eisenberg D (2010) J Biol Chem 285:29671–29675
28. Apostol MI, Wiltzius JJW, Sawaya MR, Cascio D, Eisenberg D (2011) Biochemistry 50:2456–2463
29. Tran HT, Mao A, Pappu RV (2008) J Am Chem Soc 130:7380–7392
30. Shaw DE, Maragakis P, Lindorff-Larsen K, Piana S, Dror RO, Eastwood MP, Bank JA, Jumper JM, Salmon JK, Shan YB, Wriggers W (2010) Science 330:341–346
31. Lindorff-Larsen K, Piana S, Dror RO, Shaw DE (2011) Science 334:517–520
32. Santo KP, Berjanskii M, Wishart DS, Stepanova M (2011) Prion 5:188–200
33. Bari MA, Chianini F, Vaccari G, Esposito E, Conte M, Eaton SL, Hamilton S, Finlayson J, Steele PJ, Dagleish MP, Reid HW, Bruce M, Jeffrey M, Agrimi U, Nonno R (2008) J Gen Viro 89:2975–2985
34. Humphrey W, Dalke A, Schulten K (1996) J Mol Graph Model 14:33–38
35. Jorgensen WL, Chandrasekhar J, Madura JD, Impey RW, Klein ML (1983) J Chem Phys 79:926–935
36. Kale L, Skeel R, Bhandarkar M, Brunner R, Gursoy A, Krawetz N, Phillips J, Shinozaki A, Varadarajan K, Schulten K (1999) J Comput Phys 151:283–312
37. MacKerell AD, Bashford D, Bellott M, Dunbrack RL, Evanseck JD, Field MJ, Fischer S, Gao J, Guo H, Ha S, Joseph-McCarthy D, Kuchnir L, Kuczera K, Lau FTK, Mattos C, Michnick S, Ngo T, Nguyen DT, Prodhom B, Reiher WE, Roux B, Schlenkrich M, Smith JC, Stote R, Straub J, Watanabe M, Wiorkiewicz-Kuczera J, Yin D, Karplus M (1998) J Phys Chem B 102:3586–3616
38. EI-Bastawissy E, Knaggs MH, Gilbert IH (2001) J Mol Graph Model 20:145–154
39. Kundu S, Roy D (2008) J Mol Graph Model 27:88–94
40. Xu XJ, Su JG, Chen WZ, Wang CX (2011) J Biomol Struct Dyn 28:717–727
41. Connolly ML (1983) Science 221:709–713
42. Sheinerman FB, Brooks CL (1998) J Mol Biol 278:439–456
43. Guo J, Ning L, Ren H, Liu L, Yao X (2012) Biochim Biophys Acta 1820:116–123
44. Garcia FL, Zahn R, Riek R, Wuthrich K (2000) Proc Natl Acad Sci USA 97:8334–8339
45. Chen W, van der Kamp MW, Daggett V (2010) Biochemistry 49:9874–9881
46. Hornemann S, Glockshuber R (1998) Proc Natl Acad Sci USA 95:6010–6014
47. Swietnicki W, Morillas M, Chen SG, Gambetti P, Surewicz WK (2000) Biochemistry 39:424–431
48. Zhang H, Stockel J, Mehlhorn I, Groth D, Baldwin MA, Prusiner SB, James TL, Cohen FE (1997) Biochemistry 36:3543–3553
49. Jackson GS, Hosszu LLP, Power A, Hill AF, Kenney J, Saibil H, Craven CJ, Waltho JP, Clarke AR, Collinge J (1999) Science 283:1935–1937
50. van der Kamp MW, Daggett V (2010) Biophys J 99:2289–2298